Materials Characterization 96 (2014) 135–141

Contents lists available at ScienceDirect

Materials Characterization

journal homepage: www.elsevier.com/locate/matchar

Friction stir welding of as-extruded Mg–Al–Zn alloy with higher Al content. Part II: Influence of precipitates

J. Yang, D.R. Ni, D. Wang, B.L. Xiao, Z.Y. Ma *

Shenyang National Laboratory for Materials Science, Institute of Metal Research, Chinese Academy of Sciences, 72 Wenhua Road, Shenyang 110016, China

ARTICLE INFO

Article history:
Received 29 March 2014
Received in revised form 30 July 2014
Accepted 1 August 2014
Available online 2 August 2014

Keywords:
Magnesium alloys
Friction stir welding
Banded structure
Heat treatment
Mechanical properties

ABSTRACT

Extruded Mg–Al–Zn (AZ80) plates were subjected to friction stir welding at a welding speed of 100 mm·min^{-1} and a tool rotation rates of 800 rpm. Different heat treatments were conducted before or after welding with the aim to evaluate the influence of precipitates on the weld properties. The welding joint with the solution treatment before welding exhibited enhanced ductility and decreased yield strength due to the dissolution of β-$Mg_{17}Al_{12}$ and the coarsening of grains. After aging at 180 °C for 16 h, a banded structure consisting of different densities of discontinuous β-$Mg_{17}Al_{12}$ precipitates was observed in the nugget zone of both joints with or without the solution treatment before welding. The yield strength of the joint without the solution before welding increased by 30% after aging, with the elongation being decreased. The fracture behavior of the aged joints was closely related to the banded structure where the crack propagated more easily along the coarse discontinuously precipitated bands.

1. Introduction

Problems such as porosity, thermal cracks, and oxidization often occur in the conventional fusion welding of Mg alloys. This limits the commercial applications of the Mg alloys. Friction stir welding (FSW), an innovative solid state joining technique based on plastic deformation principle [1], can effectively reduce the defects in the conventional fusion welded joints. On the other hand, the Mg alloys could exhibit a good deformability at high temperatures [2]; therefore, FSW is a promising method for joining the Mg alloys. The last decade saw more and more reports on the FSW of Mg alloys [3–19].

Nowadays most of research efforts of FSW Mg alloys were focused on the AZ series alloys, especially on those with lower Al content (AZ31 and AZ61) [3–10]. For the AZ31 alloy, sound FSW joints could be produced especially at a higher heat input [4–6], and a joint efficiency as high as 95% could be achieved [4,6]. Furthermore, it was reported that the tensile properties of FSW AZ31 joints were affected by both grain size and texture distribution of the welds [3–10]. In particular, the fracture behavior of the joints was related to the texture distribution [8–10].

For the Mg alloys with higher Al content, such as AZ80 and AZ91, most of the FSW studies [11–13] were focused on the as-cast alloys [11,20], and FSW joints with high joint efficiency could be obtained [12]. During tension, these joints tended to fracture in the part of the parent material (PM) due to its coarse microstructure as well as casting defects.

For the wrought (rolled or extruded) Mg alloys with higher Al content, their strength and ductility are significantly improved due to smaller grains and fewer coarse β-$Mg_{17}Al_{12}$ particles [21–23]. In Part I, the present authors conducted FSW of as-extruded AZ80 at a welding speed of 100 mm·min^{-1} and tool rotation rates of 400–1200 rpm. It was revealed that the as-extruded AZ80 exhibited a markedly different weldability from the AZ31 alloy, and a joint efficiency of 92% was achieved at 800 rpm with the joint fracturing in the nugget zone (NZ) during tension. This implies that the joint could be further strengthened by increasing the strength of the NZ.

Our previous study showed that the β precipitates greatly affected the strength and fracture behavior of Mg alloys with higher Al content (AZ91D) [24]. Cracks occurred preferentially within the coarse β-$Mg_{17}Al_{12}$ particles in the as-cast alloy during fatigue test. However, for the friction stir processed and subsequently aged sample, the uniformly distributed fine β precipitates could decrease the possibility of crack initiation and restrain the propagation of cracks, thereby increasing the fatigue strength greatly. Based on above reasons, a proper heat treatment prior to and/or after FSW is necessary to investigate the effect of the β precipitates on the weldability and mechanical properties of the as-extruded AZ80.

In this study, extruded AZ80 plates were subjected to FSW investigation at a tool rotation rate of 800 rpm and a traverse speed of 100 mm·min^{-1}. This parameter was selected based on the optimum results obtained in Part I. Different heat treatments were conducted prior

* Corresponding author.
E-mail address: zyma@imr.ac.cn (Z.Y. Ma).

http://dx.doi.org/10.1016/j.matchar.2014.08.001
1044-5803/

to or after FSW to carefully evaluate the effect of the β precipitates on the weld properties of the Mg–Al–Zn alloy with high Al content.

2. Material and Methods

AZ80 extruded plates with a nominal composition of 8.00Al–0.33Zn–0.25Mn–0.036Si–0.0018Cu–0.0012Ni–0.0016Fe (wt.%,) were used in this study. 6-mm-thick plates were friction stir welded along the extrusion direction at a traverse speed of 100 mm·min^{-1} and a rotation rate of 800 rpm (the best parameter in Part I). A tool with a concave shoulder 20 mm in diameter and a threaded conical pin 8 mm in root diameter, 6.2 mm in tip diameter and 5.7 mm in length was used. The FSW was performed under the plunge control model and the plunge depth was fixed at 0.15 mm. The tilt angle for all welds was maintained at 2.7°. Three different heat treatments were conducted on the PM and FSW joints (Table 1): (i) a post-FSW aging at 180 °C for 16 h (denoted by FSW-A), (ii) a pre-FSW solution treatment at 410 °C for 6 h (denoted by S-FSW), and (iii) a pre-FSW solution treatment plus a post-FSW aging at 180 °C for 16 h (denoted by S-FSW-A). The solution and aging treatments are routinely used for industrial processing of AZ80 alloys.

The process and parameters of FSW, preparation of optical microscopic (OM), scanning electron microscopic (SEM), and transmission electron microscopic (TEM) specimens, and tests of microhardness and tension were described in detail in Part I.

3. Results and Discussion

3.1. Microstructural Characteristics

3.1.1. FSW-A Sample

In Part I, the banded structure resulting from different Al concentrations was observed in the NZ of the FSW joint. For the FSW-A joint, the banded structure became more obvious in the NZ (Fig. 1a). It was noted that the β phase precipitated from the supersaturated solution in the PM with two types of precipitation: discontinuous precipitation (DP) and continuous precipitation (CP) (Fig. 1b), which are the two kinds of generally accepted precipitation in the AZ80 alloy during aging [25]. In the NZ, the banded structures were observed both in the transverse direction (TD) (Fig. 1c) and the longitudinal direction (LD) (Fig. 1d). In particular, it was detected that the band spacing (112.6 μm) corresponded very closely to the value of ν/ω (tool advance per revolution, ν is welding speed and ω is rotational rate) in the LD.

High-magnification micrographs show the bands with different DP densities (Fig. 1e). The bands with high DP density were named as DP bands, while the bands with low DP density were detected to have many CP in the grains among DP (not shown in this paper) and called CP bands. However, the CP was too fine, so that it was difficult to exhibit the CP in the CP band at low magnification.

TEM examinations showed microstructures in the NZ for the FSW-A joint (Fig. 2). Fig. 2a and b was taken from the grains with high and low DP densities, respectively, in which the DP with lamellar and globular shapes was the predominant precipitation (Fig. 2a) and mainly precipitated at the grain boundaries (Fig. 2b). Besides, the fine CP laths were mainly distributed within the grains (Fig. 2b). It was also noticed that the fine CP laths were surrounded by a high density of dislocations but the DP had few dislocations (Fig. 2a and b). Fig. 2c further shows dislocation tangles in the NZ. In addition, some Al_6Mn compound particles were also found at the grain boundaries, indicating that these particles could not be fully dissolved during FSW (Fig. 2d).

Table 1
Heat treatments for FSW AZ80 joints.

No.	Sample	Heat treatment
1	FSW	–
2	FSW-A	FSW + aging (180 °C/16 h)
3	S-FSW	Solution (410 °C/6 h) + FSW
4	S-FSW-A	Solution (410 °C/6 h) + FSW + aging (180 °C/16 h)

3.1.2. S-FSW Sample

The pre-FSW solution treatment at 410 °C for 6 h on the as-extruded AZ80 (Fig. 3a) caused obvious grain coarsening (Table 2, from 16.2 to 37.8 μm) and the dissolution of most β phases (Fig. 3b). After FSW, the microstructure of the NZ was characterized by fine and uniform recrystallized grains with an average size of 25.8 μm (Fig. 3c, Table 2). Also, no heterogeneous structure nor a banded structure was found in the NZ of the S-FSW joint. Larger equiaxed grains were observed in the thermo-mechanically affected zone (TMAZ) (Fig. 3d), but nearly no β phases were detected in both the NZ and TMAZ of the S-FSW joint.

The grain size of the NZ in the S-FSW joint was refined but larger than that in the NZ of the FSW joint (Table 2, 14.4 μm). The ratio of d_{NZ}/d_{PM} was used to identify the grain refinement degree, which was 0.88 for the FSW joint and 0.69 for the S-FSW joint (Table 2). This indicates that the degree of grain refinement in the S-FSW joint was much larger than that in the FSW joint. This discrepancy should be related to the solution-treated plate that showed a lower initial hardness than the as-extruded counterpart, with the average initial hardness for the solution-treated and as-extruded plate being about 60.6 and 72.3 Hv, respectively. Therefore, the material flow resistance experienced in the S-FSW joint was a little lower, resulting in a higher strain rate and a lower temperature [26]. The influence of strain rate and temperature under hot working conditions is often incorporated in Z-parameter ($\dot{\varepsilon} \times \exp(Q / RT)$) for magnesium alloys [27]. Usually, the higher strain rate and lower deformation temperature mean higher Z value, and thus smaller recrystallization grains could be obtained after the short FSW process [26]. However, the coarser initial grains in the PM influenced the grain size in the NZ for the S-FSW joint [28]. So, although the S-FSW joint exhibited the larger degree of grain refinement in the NZ, it had a larger grain size in the NZ.

3.1.3. S-FSW-A Sample

For the S-FSW-A joint, the aging resulted in the generation of the banded structure with different DP densities in the NZ (Fig. 4a), which was similar to that in the FSW-A joint (Fig. 1c). However, the banded structure in the S-FSW-A joint was less distinct than that in the FSW-A joint. It was noted that the DP in the CP bands in the S-FSW-A joint (Fig. 4b) was more than that in the FSW-A joint (Fig. 1e). In addition, the main precipitate was the DP in the DP band for the S-FSW-A joint (Fig. 4c).

3.1.4. Formation of Banded Structure

The banded structure was observed in the NZ of the FSW (Part I), FSW-A (Fig. 1) and S-FSW-A joints (Fig. 4) but not in the S-FSW joint (Fig. 3). In previous FSW studies, the generation of banded structures has been explained by the texture [29], welding tool geometrical effect [30], particle-rich bands, the variation in grain size [31], and strain gradient [32]. However, in the present study the origin of the banded structure might be different in the joints with different heat treatments.

In the FSW joint, the banded structure was revealed as the alternating regions of high and low Al concentrations (Part I). After the post-FSW aging, the banded structure became more obvious in the NZ (Fig. 1a), with the alternation of CP bands and DP bands (Fig. 1c). It should be noted that the banded structure obtained by aging is different from that in other FSW studies [29–32]. To explain the different precipitation rates of CP and DP in the NZ, several reasons mentioned above were taken into account. Firstly, the texture variation could not cause different precipitation rates between the CP and DP, because the same predominant orientation relationship between β (p) and matrix (m) was found for both the CP and DP [33]. Secondly, no obvious grain size variation was observed in the NZ. Other explanations like particle-rich bands and geometrical effect had no direct relationship with the different precipitation rates.

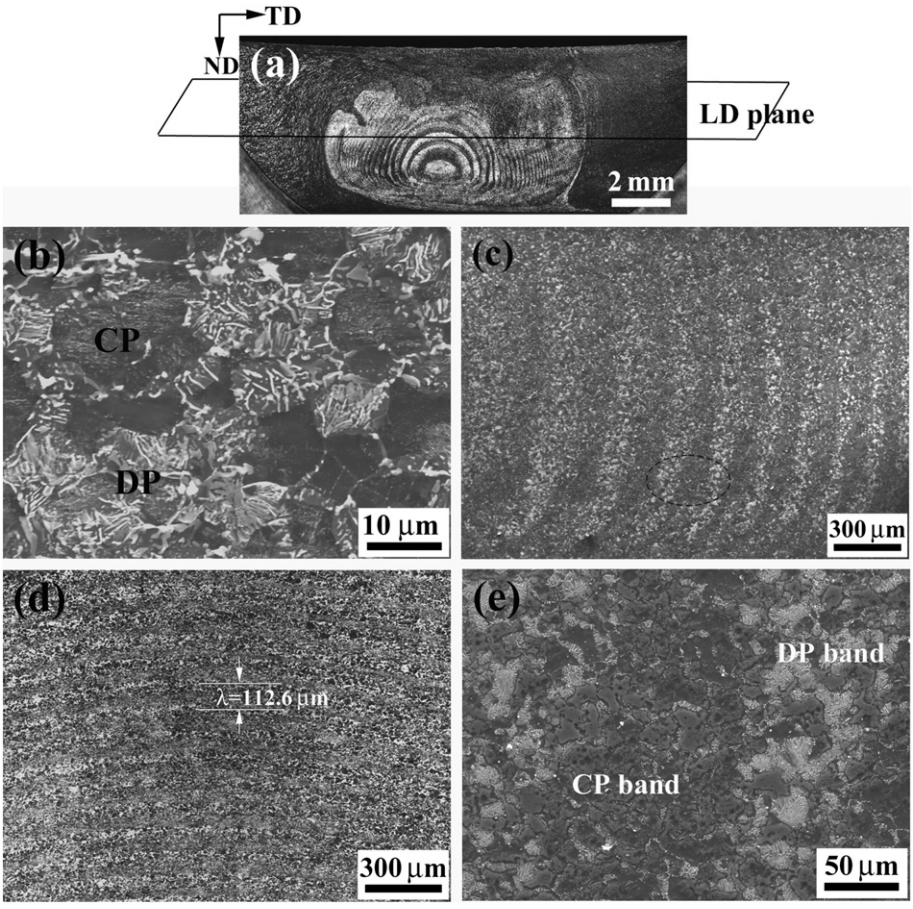

Fig. 1. (a) Macrographs of NZ in FSW-A joint, (b) DP and CP in PM, (c) and (d) banded structure on transverse and longitudinal sections of NZ, and (e) magnified image of selected region as shown by an ellipse in (c). (ND: normal direction, TD: transverse direction, LD: longitudinal direction & welding direction).

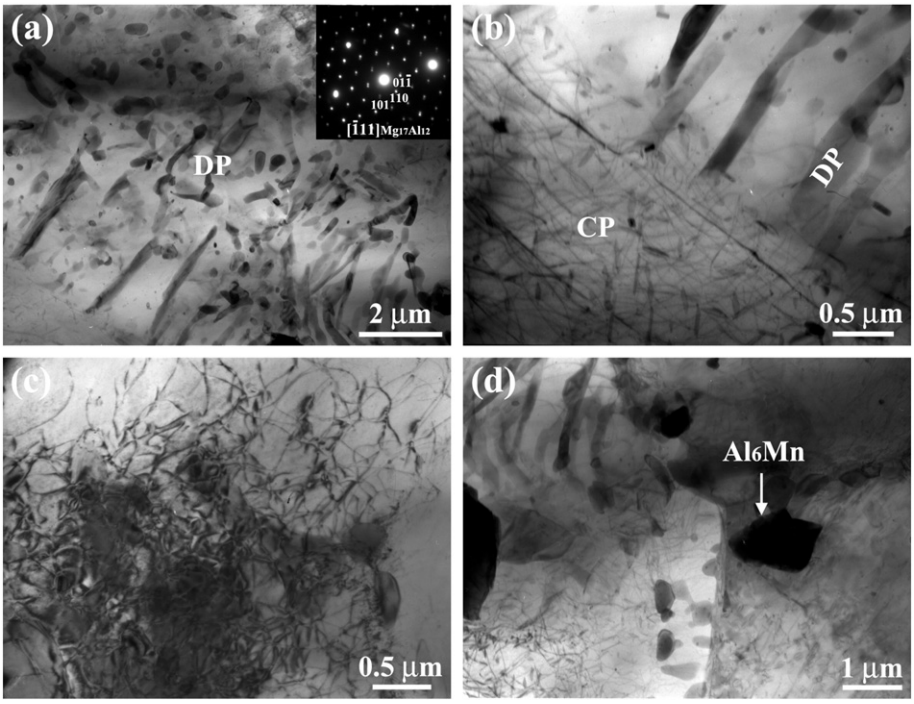

Fig. 2. TEM images of NZ of FSW-A joint: (a) DP, (b) DP and CP, (c) dislocation tangle, and (d) Al_6Mn phase.

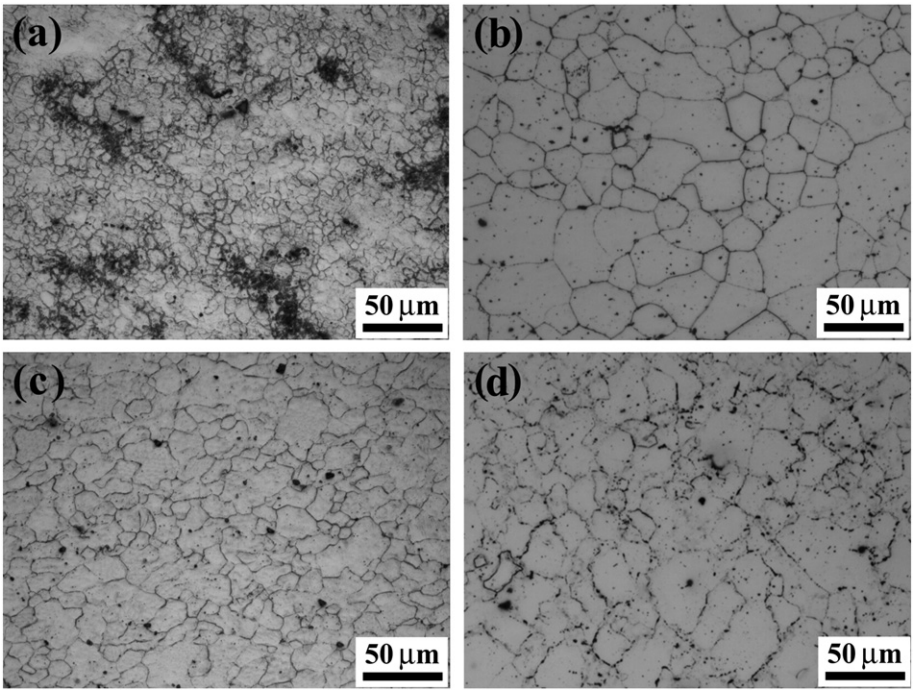

Fig. 3. Microstructures of (a) extruded PM and (b)–(d) S-FSW joint: (b) pre-solutionized PM, (c) NZ, and (d) TMAZ.

However, the strain could affect the formation of the banded structure by influencing the precipitation rate of the CP in the FSW-A joint. It was reported that the strain was a remarkable driving force for the CP, which could increase the nucleation of the CP and accelerate the growth of precipitates [34]. This is consistent with the present result with high dislocation density in the CP band (Fig. 2b). In the FSW joint, special distributions of strain were reported by the computed and experimental results [32,35,36]. Xu and Deng [32] pointed out that there were periodically alternating bands of high and low equivalent plastic strains on the longitudinal plane and the spacing between the bands closely matched the distance of the tool advance per revolution. As a result, the CP could rapidly form in the region of high strain, resulting in a rapid relief of supersaturation, thus eliminating the driving force for the DP. Within the whole NZ, the CP densities could be different in the regions of different strains, leading to the formation of the banded structure.

In addition, the chemical factor should be taken into account to explain the banded structure in the FSW-A joint. The Al content had different effects on the precipitation of DP and CP. The precipitation of DP has vital relationship with Al content [34]: it initiated at the grain boundaries with the aggregation of the Al solutes, and then grew to the inside of grains and made the matrix depleted in the Al solutes. Finally, it stopped growing due to the decrease in the Al content. However, the generation of CP was not sensitive to the fluctuation of the Al concentration. In the FSW joint, the Al concentration fluctuated in the banded structure. Therefore, when the aging was conducted, the precipitation rates of DP should be different in various regions. The zone with a higher Al concentration in the matrix promoted the generation of DP, while the lower Al concentration suppressed the development of DP. Consequently, the DP occupied most of grains in the DP bands, but only precipitated at the grain boundaries in the CP bands (Fig. 1e).

Table 2
Grain sizes (d) in PM and NZ of FSW AZ80 and S-FSW AZ80 joints.

Sample	FSW		S-FSW	
	PM	NZ	PM	NZ
d, μm	16.2	14.4	37.8	25.8
d_{NZ}/d_{PM}	0.88		0.69	

Therefore, the banded structure in the FSW-A joint resulted from the strain distribution and the fluctuation of Al concentration in the NZ. The former was the inherent characteristic during FSW and was also found in other alloys [35,36], while the latter was related to the parent material.

In the S-FSW joint, however, the banded structure was not observed. Since the pre-FSW solution resulted in the disappearance of the β phase and the heterogeneous structures in the PM, a uniform distribution of Al concentration was produced in the Mg matrix. Therefore, after FSW, the fluctuation of Al concentration could not be formed in the NZ and thus the banded structure was eliminated.

In the S-FSW-A joint (Fig. 4), the reasons for the banded structure were different from that in the FSW-A joint (Fig. 3), because of the elimination of the fluctuation of the Al concentration in the S-FSW joint. However, the strain gradient [32,35,36] still existed in the S-FSW joint, which could influence the precipitation rate of CP during post-FSW aging [34]. Therefore, bands with different CP densities were produced after aging, forming the banded structure in the S-FSW-A joint. Furthermore, the precipitation rate of DP had little variation between the bands, because the Al concentration fluctuation was eliminated.

3.2. Microhardness

Fig. 5 shows the hardness profiles of various FSW joints along the mid-thickness of the joints. For the FSW joint, the hardness value in the NZ was lower than that in the PM, and this was attributed to the dissolution of β phase. After post-FSW aging, with the precipitation of β phase, the hardness of both the PM and the NZ increased with the latter having a hardness increase of 12 HV over that of the FSW joint. Furthermore, the PM and NZ of the FSW-A joint exhibited similar hardness values and this should be attributed to the similar precipitation hardening effect of the β phase. This implies that the hardness improvement after aging was less in the PM than in the NZ, attributable to the lower Al concentration in the matrix of the PM.

When the pre-FSW solution was conducted, the hardness of the S-FSW joint obviously decreased compared to that of the FSW joint, and this is due to the fundamental dissolution of the β phase throughout the entire joint. Besides, the hardness value had little difference

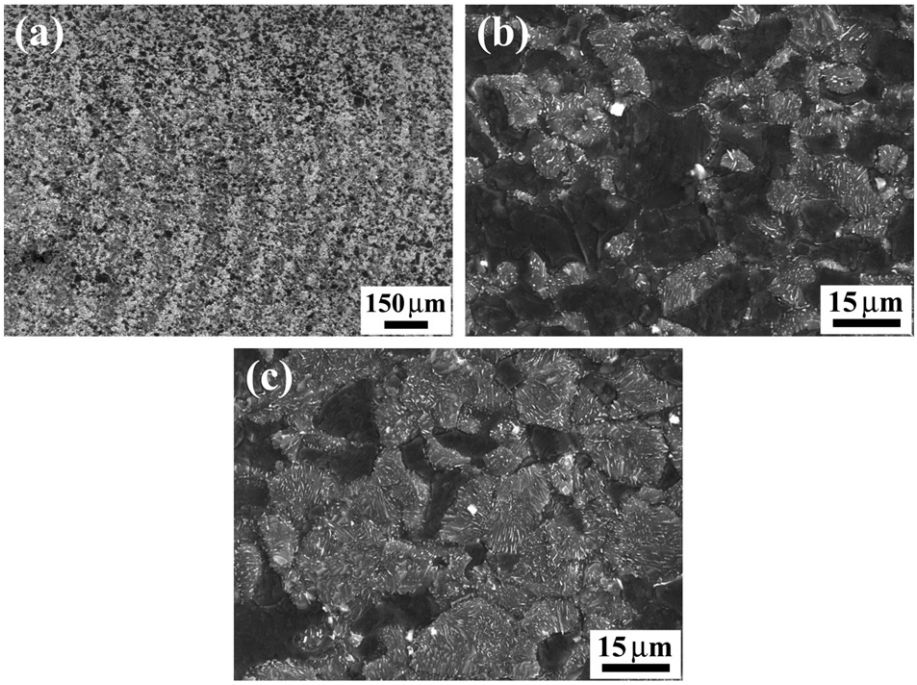

Fig. 4. Microstructures of S-FSW-A joint: (a) banded structure, (b) band of low DP density (CP band), and (c) band of high DP density (DP band).

between the NZ and the PM in spite of the variation in the grain size, which was similar to the hardness profile of the FSW AZ31 due to the hardness insensitivity to the grain size variation [3,37].

After the post-FSW aging, the hardness of the S-FSW-A joint increased greatly due to the precipitation strengthening of the β phase, and a higher hardness increment was detected in the S-FSW-A joint than in the FSW-A joint for the higher Al concentration in the matrix. Moreover, little hardness difference was found between the NZ and PM due to similar Al concentrations of the NZ and PM in the S-FSW joint. Also, it was noted that similar hardness profiles were found in the FSW-A and S-FSW-A joints, which could be attributed to the similar aging strengthening effect.

3.3. Tensile Properties

The tensile properties of the FSW joints at different heat treatments are shown in Table 3. The FSW joint showed a UTS of 304 MPa and a YS of 161 MPa with an elongation of 11.5%. The post-FSW aging (FSW-A) resulted in significant improvement of the YS (210 MPa, increased by 30%), a slight decrease of UTS (296 MPa) and an obvious decrease of the elongation (5.7%). However, similar UTS and elongation were obtained for the FSW and S-FSW joints, but a lower YS (146 MPa) was observed for the S-FSW joint. After post-FSW aging the S-FSW-A joint exhibited increased YS (169 MPa) but significantly decreased elongation (4.0%).

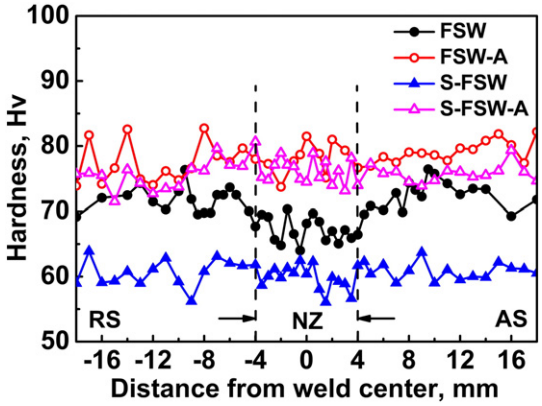

Fig. 5. Hardness profiles of FSW AZ80 joints at various heat treatments.

Both the grain size and the precipitates could influence the YS. For Mg–Al alloys with a small quantity of precipitates, basal slip and {1012} twinning are the principal deformation modes [34], and the grain refinement is a primary method of improving the YS in these alloys. Under the aging condition, the precipitation of β could break up the basal slip and generate cross slip and dislocation tangle [34], thus increasing the YS dramatically [22,38] but decreasing the ductility [39]. In the S-FSW joint, few β phases and larger grains in the NZ decreased the YS from 161 MPa to 146 MPa. After aging, due to the precipitation strengthening, the YS of the FSW-A joint increased by 49 MPa compared to that of the FSW joint and the YS of the S-FSW-A joints increased by 23 MPa compared to that of the S-FSW joint. However, for the S-FSW-A joint, the grain size in both the PM and NZ was larger than that for the FSW-A joint, leading to a lower YS than that of the FSW-A joint.

On the other hand, it is noted that the UTS of the FSW joints varied little. The FSW joint showed a lower UTS compared to the PM due to the dissolution of the β precipitates. For the S-FSW joint, the UTS was also kept about 300 MPa because of the solid solution strengthening [38]. The UTS of both the FSW-A and S-FSW-A joints had no improvement and this should be mainly attributed to the β precipitates and the banded structure. The DP was large and brittle and prone to crack during tension [21], while the fine CP was not oriented to block the basal slip effectively [33,34]. Therefore, the aging treatment had a weaker influence on the UTS for the AZ80 and AZ91 alloys [22], though a large increase of YS could be obtained [22,38]. Also, the banded structure also decreased the UTS by promoting the

Table 3
Tensile properties of FSW AZ80 joints at various heat treatments.

Sample	YS, MPa	UTS, MPa	El. %	Fracture location
Extruded PM	179.4 ± 5.2	330.0 ± 3.4	22.6 ± 0.9	–
FSW	160.8 ± 0.5	304.5 ± 1.9	11.5 ± 0.3	NZ
FSW-A	209.6 ± 0.7	295.7 ± 1.9	5.7 ± 0.1	Boundary of NZ
S-FSW	145.8 ± 1.1	301.4 ± 1.5	12.3 ± 0.1	TMAZ
S-FSW-A	168.6 ± 0.8	308.5 ± 10	4.0 ± 2.0	Boundary of NZ

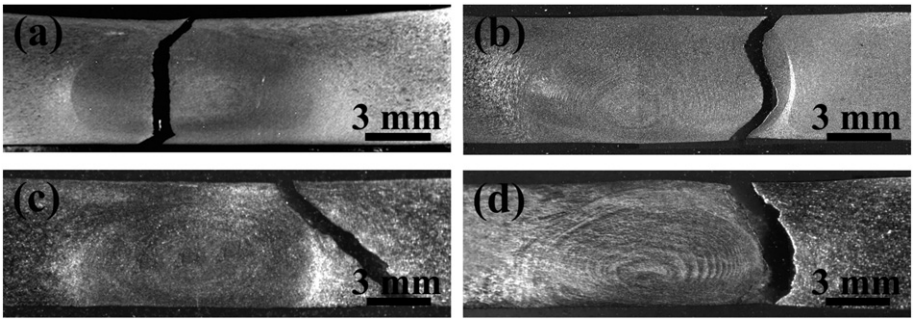

Fig. 6. Macrographs of cross section of fractured joints with different heat treatments: (a) FSW, (b) FSW-A, (c) S-FSW, and (d) S-FSW-A.

crack propagation along the DP bands. For the above two reasons, the UTS of the FSW AZ80 joints did not increase after aging, but the ductility decreased significantly.

The heat treatments changed the fracture behavior of the FSW joints (Fig. 6). The FSW joint failed in the NZ (Fig. 6a), which was consistent with the lowest hardness region (Fig. 5). While the fracture location shifted to the boundary of the NZ after the post-FSW aging (Fig. 6b). For the S-FSW joint, the joint failed in the region around the TMAZ (Fig. 6c). This is similar to the FSW AZ61 [7,8] and was attributed to the highest Schmid factor in the TMAZ. The fracture was still at the boundary of the NZ after the post-FSW aging (Fig. 6d).

Both FSW-A and S-FSW-A joints failed at the boundary of NZ, and this could be attributed to the banded structure. The microstructure on the cross-sectional plane of the failed FSW-A joint showed that the DP bands at the NZ boundary were the fracture location (Fig. 7a). A high magnification micrograph shows that the crack propagated along the DP (Fig. 7b). Similar results were also found in the S-FSW-A joint (not shown). It was reported that the $Mg/Mg_{17}Al_{12}$ interface acted as the crack initiation and cracks were prone to propagating along the coarse $Mg_{17}Al_{12}$ [39]. In the present study, cracks would propagate more easily along the coarse DP bands, but it was difficult to cross the fine CP bands (Fig. 7b). Besides, for the FSW-A joint, the relatively lower hardness at the NZ boundary (Fig. 5) may influence the fracture behavior.

On the fracture surface (Fig. 8), dimples and tearing ridges were found for all the FSW joints, indicating ductile fracture characteristics. For the FSW and S-FSW joints (Fig. 8a and c), a large number of deep dimples were detected and this was in agreement with their higher elongation. However, for the FSW-A and S-FSW-A joints, dimples were less and shallow, and some cleavage features occurred (Fig. 8b and d), which is consistent with their much lower elongation.

4. Conclusions

Extruded AZ80 plates were subjected to FSW at a welding speed of 100 $mm \cdot min^{-1}$ and a tool rotation rates of 800 rpm. Heat treatments both before and after welding were conducted in order to evaluate the influence of precipitates on the weld properties of the AZ80 alloy. The following conclusions can be drawn:

(1) For the FSW AZ80 joint, a banded structure consisting of different DP densities of β phase was generated in the NZ after post-FSW aging at 180 °C for 16 h.
(2) The pre-FSW solution dissolved most of β phases but coarsened the grains (37.8 μm) in the PM. After FSW, no banded structure was detected, but the refinement degree of the grains (25.8 μm) was less than that in the FSW joint (14.4 μm). The aging resulted in the generation of the banded structure with different DP densities in the NZ.
(3) For the FSW joint, the hardness of the NZ increased after aging. Compared to the FSW joint, the S-FSW one showed a lower hardness which varied little between the NZ and PM, but similar hardness profiles were observed in the FSW-A and S-FSW-A joints.
(4) Although similar strength and elongation were observed for the FSW and S-FSW joints, the latter exhibited a slightly lower YS. Both the joints exhibited increased YS but reduced elongation after post-FSW aging. The fracture of the aged joints was related to the banded structure because cracks would propagate more easily along the coarse DP bands.

Acknowledgments

This work was supported by the National Natural Science Foundation of China under Grant Nos. 51371179 and 51331008.

References

[1] R.S. Mishra, Z.Y. Ma, Friction stir welding and processing, Mater. Sci. Eng. R 50 (2005) 1–78.
[2] S.R. Agnew, O. Duygulu, Plastic anisotropy and the role of non-basal slip in magnesium alloy AZ31B, Int. J. Plast. 21 (2005) 1161–1193.
[3] J. Yang, B.L. Xiao, D. Wang, Z.Y. Ma, Effects of heat input on tensile properties and fracture behavior of friction stir welded Mg–3Al–1Zn alloy, Mater. Sci. Eng. A 527 (2010) 708–714.

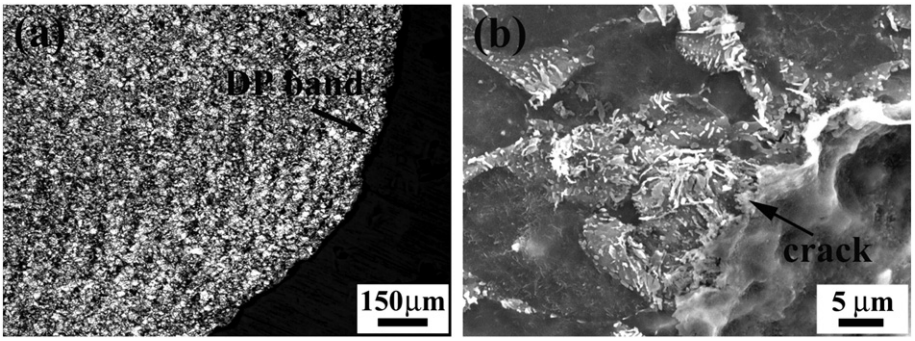

Fig. 7. Microstructure of failed FSW-A joint in cross-sectional plane: (a) crack propagation along DP band, and (b) magnified image.

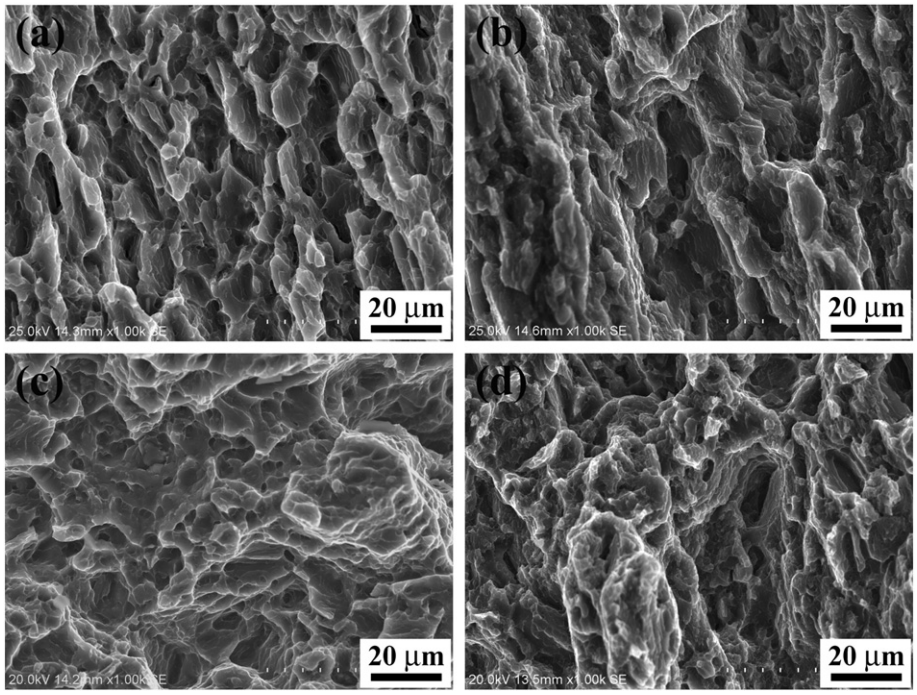

Fig. 8. SEM fractographs of FSW AZ80 joints at different heat treatments: (a) FSW, (b) FSW-A, (c) S-FSW, and (d) S-FSW-A.

[4] J. Yang, D. Wang, B.L. Xiao, D.R. Ni, Z.Y. Ma, Effects of rotation rates on microstructure, mechanical properties, and fracture behavior of friction stir-welded (FSW) AZ31 magnesium alloy, Metall. Mater. Trans. A 44 (2013) 517–530.
[5] L. Commin, M. Dumont, J.E. Masse, L. Barrallier, Friction stir welding of AZ31 magnesium alloy rolled sheets: influence of processing parameters, Acta Mater. 57 (2009) 326–334.
[6] M. Abbasi Gharacheh, A.H. Kokabi, G.H. Daneshi, B. Shalchi, R. Sarrafi, The influence of the ratio of "rotational speed/traverse speed" (ω/v) on mechanical properties of AZ31 friction stir welds, Int. J. Mach. Tools Manuf. 46 (2006) 1983–1987.
[7] W.B. Lee, Y.M. Yeon, S.B. Jung, Joint properties of friction stir welded AZ31B-H24 magnesium alloy, Mater. Sci. Technol. 19 (2003) 785–790.
[8] S.H.C. Park, Y.S. Sato, H. Kokawa, Basal plane texture and flow pattern in friction stir weld of a magnesium alloy, Metall. Mater. Trans. A 34A (2003) 987–994.
[9] S.H.C. Park, Y.S. Sato, H. Kokawa, Effect of micro-texture on fracture location in friction stir weld of Mg alloy AZ61 during tensile test, Scr. Mater. 49 (2003) 161–166.
[10] J. Yang, D. Wang, B.L. Xiao, Z.Y. Ma, J. Yang, D. Wang, B.L. Xiao, Z.Y. Ma, The microstructure and mechanical properties of friction stir welded Mg–3Al–1Zn alloy at high rotation rates, 8th Inter Friction Stir Welding Symp, Timmendorfer Strand, Germany, 2010.
[11] S.H.C. Park, Y.S. Sato, H. Kokawa, Microstructural evolution and its effect on Hall–Petch relationship in friction stir welding of thixomolded Mg alloy AZ91D, J. Mater. Sci. 38 (2003) 4379–4383.
[12] W.B. Lee, J.W. Kim, Y.M. Yeon, S.B. Jung, The joint characteristics of friction stir welded AZ91D magnesium alloy, Mater. Trans. 44 (2003) 917–923.
[13] W.P. Xu, L. Xing, L.M. Ke, Analysis of the grain orientation and texture of friction stir welded magnesium alloy, Mater. Sci. Forum 620–622 (2009) 97–100.
[14] G.M. Xie, Z.Y. Ma, L. Geng, Effect of microstructural evolution on mechanical properties of friction stir welded ZK60 alloy, Mater. Sci. Eng. A 486 (2008) 49–55.
[15] D.T. Zhang, M. Suzuki, K. Maruyama, Microstructural evolution of a heat-resistant magnesium alloy due to friction stir welding, Scr. Mater. 52 (2005) 899–903.
[16] G.M. Xie, Z.Y. Ma, L. Geng, R.S. Chen, Microstructural evolution and mechanical properties of friction stir welded Mg–Zn–Y–Zr alloy, Mater. Sci. Eng. A 471 (2007) 63–68.
[17] J.A. Esparza, W.C. Davis, L.E. Murr, Microstructure-property studies in friction-stir welded, thixomolded magnesium alloy AM60, J. Mater. Sci. 38 (2003) 941–952.
[18] G.M. Xie, Z.Y. Ma, L. Geng, Effect of Y addition on microstructure and mechanical properties of friction stir welded ZK60 alloy, J. Mater. Sci. Technol. 25 (2009) 351–355.
[19] G.M. Xie, Z.Y. Ma, L. Geng, Effects of friction stir welding parameters on microstructures and mechanical properties of ZK60 magnesium alloy joints, Acta Metall. Sin. 44 (2008) 665–670.
[20] A.H. Feng, B.L. Xiao, Z.Y. Ma, R.S. Chen, Effect of friction stir processing procedures on microstructure and mechanical properties of Mg–Al–Zn casting, Metall. Mater. Trans. A 40A (2009) 2447–2456.
[21] Y. Liu, Y.Y. Li, D.T. Zhang, T.W.L. Ngai, W. Chen, Microstructure and properties of AZ80 magnesium alloy prepared by hot extrusion from recycled machined chips, Trans. Nonferrous Met. Soc. China 12 (2002) 882–885.
[22] A.H. Feng, Z.Y. Ma, Enhanced mechanical properties of Mg–Al–Zn cast alloy via friction stir processing, Scr. Mater. 56 (2007) 397–400.
[23] D.G.L. Prakash, D. Regener, Quantitative characterization of $Mg_{17}Al_{12}$ phase and grain size in HPDC AZ91 magnesium alloy, J. Alloys Compd. 461 (2008) 139–146.
[24] D.R. Ni, D. Wang, A.H. Feng, G. Yao, Z.Y. Ma, Enhancing the high-cycle fatigue strength of Mg–9Al–1Zn casting by friction stir processing, Scr. Mater. 61 (2009) 568–571.
[25] D. Duly, J.P. Simon, Y. Brechet, On the competition between continuous and discontinuous precipitations in binary Mg–Al alloys, Acta Metall. Mater. 43 (1995) 101–106.
[26] C.I. Chang, C.J. Lee, J.C. Huang, Relationship between grain size and Zener–Holloman parameter during friction stir processing in AZ31 Mg alloys, Scr. Mater. 51 (2004) 509–514.
[27] S.W. Xu, S. Kamado, T. Honma, Recrystallization mechanism and the relationship between grain size and Zener–Hollomon parameter of Mg–Al–Zn–Ca alloys during hot compression, Scr. Mater. 63 (2010) 293–296.
[28] F.J. Humphreys, M. Hatherly, Recrystallization and Related Annealing Phenomena, 2nd ed. Elsevier Ltd., Netherlands, 2004.
[29] J.A. Schneider, A.C. Nunes, Characterization of plastic flow and resulting microtextures in a friction stir weld, Metall. Mater. Trans. B 35 (2004) 777–783.
[30] K.N. Krishnan, On the formation of onion rings in friction stir welds, Mater. Sci. Eng. A 327 (2002) 246–251.
[31] M.A. Sutton, B. Yang, A.P. Reynolds, R. Taylor, Microstructural studies of friction stir welds in 2024-T3 aluminum, Mater. Sci. Eng. A 323 (2002) 160–166.
[32] S.W. Xu, X.M. Deng, A study of texture patterns in friction stir welds, Acta Mater. 56 (2008) 1326–1341.
[33] S. Celotto, TEM study of continuous precipitation in Mg–9 wt.%Al–1 wt.%Zn alloy, Acta Mater. 48 (2000) 1775–1787.
[34] J.B. Clark, Age hardening in a Mg–9 wt percent Al alloy, Acta Metall. 16 (1968) (141–&).
[35] Ø. Frigaard, Ø. Grong, O.T. Midling, A process model for friction stir welding of age hardening aluminum alloys, Metall. Mater. Trans. A 32A (2001) 1189–1200.
[36] A. Arora, R. Nandan, A.P. Reynolds, T. DebRoy, Torque, power requirement and stir zone geometry in friction stir welding through modeling and experiments, Scr. Mater. 60 (2009) 13–16.
[37] W. Woo, H. Choo, M.B. Prime, Z. Feng, B. Clausen, Microstructure, texture and residual stress in a friction-stir-processed AZ31B magnesium alloy, Acta Mater. 56 (2008) 1701–1711.
[38] C.H. Caceres, C.J. Davidson, J.R. Griffiths, C.L. Newton, Effects of solidification rate and ageing on the microstructure and mechanical properties of AZ91 alloy, Mater. Sci. Eng. A 325 (2002) 344–355.
[39] Y.Z. Lu, Q.D. Wang, W.J. Ding, X.Q. Zeng, Y.P. Zhu, Fracture behavior of AZ91 magnesium alloy, Mater. Lett. 44 (2000) 265–268.